Numerical study of rigid and flexible wing shapes in hover

Aamer Shahzad, Fang-Bao Tian, John Young and Joseph C S Lai

School of Engineering and Information Technology, the University of New South Wales, Canberra, ACT, 2600, Australia

a.shahzad@student.adfa.edu.au

Abstract. This study is focused on evaluating the aerodynamic performance of rigid and isotropic flexible wing shapes defined by the radius of the first moment of wing area ($\bar{r_1}$) at Reynolds number of 6000. An immersed boundary method was used to solve the 3D, viscous, incompressible Navier-Stokes equations, and coupled with an in-house non-linear finite element solver for fluid structure interaction simulations. Numerical simulations of flexible $\bar{r_1}$ = 0.43, 0.53 and 0.63 wing shapes performed with a single degree of freedom flapping shows that thrust and peak lift coefficients increase with $\bar{r_1}$. Higher thrust in the $\bar{r_1}$ = 0.63 wing is attributed to the large induced pitch angle, and higher peak lift (compared to the rigid counterpart) results from an increase in the stroke amplitude and spanwise deformation of the wing that anchors the leading edge vortex.

1. Introduction

There has been a significant increase in the research interest recently to understand the inspiring flight characteristics of insects for developing insect-like flapping wing micro aerial vehicles (MAVs). Typical applications include search and rescue operations, situational awareness in the combat field, aerial reconnaissance, counter drug operations, sensing biological, nuclear, chemical agents, sports broadcasting and many more. The aerodynamic performance of flapping wings is governed by wing geometric parameters such as shape, area, aspect ratio (AR), leading edge sweep and location of pivot point. Of these, the wing shape and AR have been studied extensively in the past. Here AR is defined as the ratio of the wing span (R) to the mean chord length (c) of a wing. Phillips et al. [1] and Ozen and Rockwell [2] observed similar flow structures on generic wing shapes. While Luo and Sun [3] found a less than 10% difference in the lift of ten wing shapes based on a fruitfly's wing, clear trends have been reported by others [4, 5] . It was found that the wings with more area outboard (distributed towards the wing tip) produce higher lift at the cost of efficiency.

For MAV applications, Ansari et al. [4] recommended high AR wings with straight or almost straight leading edge (LE), and more area outboard to produce high lift. However, their quasi-steady model had limitations, as it did not take into account the spanwise flow, tip vortex and aspects of viscosity, for example, vortex diffusion and stretching. In addition, the generic wing shapes in their study have different LE sweep. For instance, rectangle, ellipse and reverse ellipse have straight, swept back and swept forward LE respectively. The LE orientation is expected to influence the formation and positioning of the leading edge vortex (LEV), and thus, the lift. The limitations of the study of Ansari et al. [4] warrant further investigation of wing shapes.

In our previous work [6], the Reynolds number (Re) effects on the performance of $\bar{r}_1$= 0.43, 0.53, 0.63 and rectangular wings with AR = 2.96 were assessed at Re = 12, 400 and 13500. Here $\bar{r}_1$, the radius of the first moment of inertia, defines the distribution of the wing area along the span of the wing. The $\bar{r}_1$= 0.43 wing is found to be the most efficient in terms of power economy (PE) and the finding is Re independent. PE represents the ratio of the mean lift coefficient to the aerodynamic power coefficient. Since previous studies [1-5] have been restricted to rigid wing shapes, this study extends the previous work [6] to investigate the effect of introducing flexibility on the performance of different wing shapes. The study is carried out at Re = 6000, representative of a hawkmoth, based on the mean chord length (c) and tip velocity (U_{tip}).

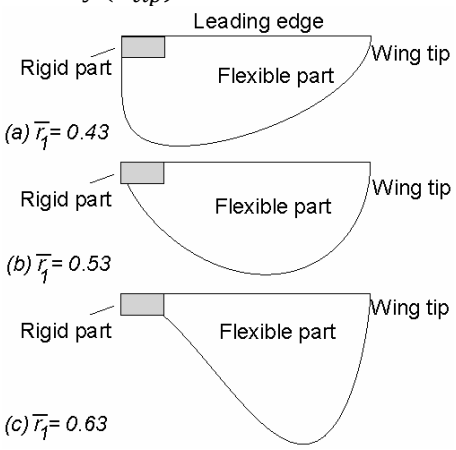

Figure 1. Flexible wing shapes with AR = 2.96.

2. Wing geometry and kinematics

The insect wings have a variety of shapes that can be reasonably approximated by the radius of the first moment of wing area ($\bar{r}_1$) using the beta distribution [7]. This distribution generates shapes with straight leading edge, constant span and area. The beta distribution shapes with AR = 2.96 for fluid structure interaction (FSI) simulations are given in figure 1.

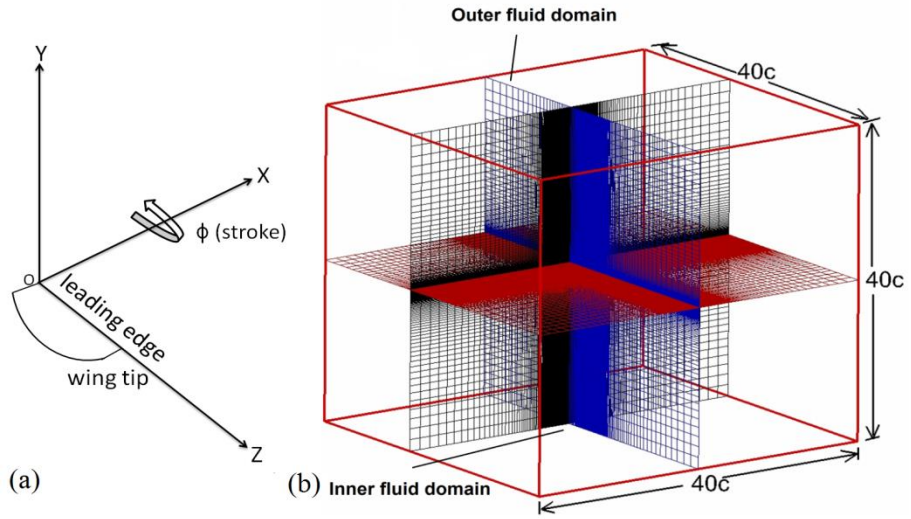

Figure 2. (a) Schematics of the wing kinematics and (b) Computational domain.

Unlike real insect wings, the $\bar{r}_1$ = 0.63 wing produced by the beta distribution has pointed wing root. The wing root is slightly modified, which brings an insignificant change (less than 3%) in AR

and the area of the wing. In addition, the modification of the wing root is not expected to influence the aerodynamic performance significantly because it is closer to the pivot point. The flexible wing shapes in figure 1 show rigid rectangular area at the intersection of wing root and LE, which constitutes approximately 4.3% of the total wing area. This is a reasonable approximation because, in insect wings, this part being closer to the pivot point is about 10^2-10^3 times more rigid than the distal area [8]. In the absence of this rigid part, $\overline{r_1}$= 0.63 wing may collapse as it will not be able to withstand high stresses at the narrow section of wing root. For rigid wing simulations, the flexible part of the wing in figure 1 is also considered rigid.

For the study, one degree of freedom (DOF) kinematics is used, where the wing flaps in a vertical stroke plane (figure 2 (a)). The flapping angle (ϕ) is defined by the sinusoidal function. The pitch and deviation angles are kept zero. The up stroke and down stroke motions are between t/T = 0-0.5 and 0.5-1.0, respectively. The wing flaps with a frequency (f) of 20 Hz and stroke amplitude of 56.35º [1].

For flexible wing shapes, we have assumed isotropic flexibility. These wings have same mass ratio (m*, in equation (1)), Poisson's ratio (ν, the ratio of transverse to axial strain) and effective stiffness (π_1, in equation (2)).

$$m^* = \rho_s h_s / \rho_f c \tag{1}$$

$$\pi 1 = E {h_s}^3 / [12 c^3 (1 - \nu^2) \rho_f {U_{tip}}^2] \tag{2}$$

Where ρ_s and ρ_f are the structural and fluid densities respectively, h_s the wing thickness, E the Young's modulus and U_{tip} the mean tip velocity. While m^* = 4.0 is representative of Hawkmoth wing [9], π_1 = 100 has been chosen to keep the frequency ratio, the ratio of the flapping frequency to the first natural frequency, of all the wings less than 0.3 so that the wing deformation is not dictated by the structural resonance in any case. It is reasonable to use ν = 0.3 for flapping wings [10].

3. Computational method

Numerical simulations are performed using a second order sharp interface immersed boundary method [11] to solve viscous, 3D, incompressible Navier–Stokes equations and the same solver is coupled with an in-house non-linear finite element solid mechanics solver for FSI simulations [11] of flexible wing cases. The computational domain is a cube with sides of 40c and the flow computed on a non-uniform Cartesian grid shown in figure 2 (b). This grid is kept fine (30 grid points per chord) in the inner fluid domain around a wing where it flaps in one complete cycle. The wing surface is meshed with triangular elements. The flow is assumed to be laminar. Neumann boundary condition for pressure and velocity (zero gradients) is applied on domain boundaries and no slip or penetration boundary condition on the wing surface. The performance of wing shapes is assessed using the time histories of lift coefficient ($C_L = 2F_L/\rho_f U^2 S$), thrust coefficient ($C_T = 2F_T/\rho_f U^2 S$), and aerodynamic power coefficient ($C_P = 2P/\rho_f U^3 S$) and their average values over 4th, 5th and 6th flapping cycles. Here F_L, F_T and P are the vertical lift force, horizontal thrust force and aerodynamic power respectively and U the mean tip velocity. The wing area (S) of approximately 0.0023m^2 has been used for all the wings. The aerodynamic power ($P = -\int \boldsymbol{F}.\boldsymbol{V}\, dS$) is determined by integrating the dot product of fluid force and local velocity over the wing surface.

4. Validation

After performing grid and time step independence studies (details not mentioned here), the validation of the fluid solver is performed against the experiment of Nagai et al. [12] using a single hind wing and the computational study of the same case by Naidu et al. [13]. Time histories of C_L given in figure 3 (a) show reasonable agreement, noting that the slightly higher peak values in Nagai et al. [12] are potentially attributable to the flexibility of the aluminium wing in the experiment. Rigid wing is used in this validation and the case of Naidu et al. [13]. There is also a reasonable agreement with the time history of C_D that was obtained from Nagai through private communication.

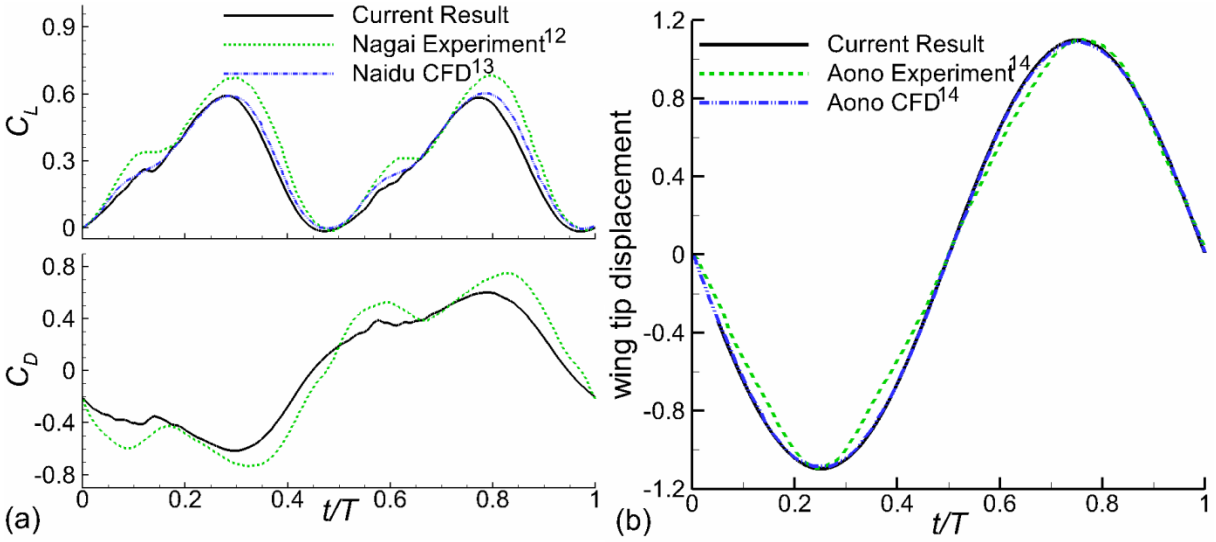

Figure 3. (a) Fluid solver validation of the time histories of C_L and C_D and (b) FSI solver validation of normalized vertical displacement of the wing tip.

FSI validation is performed against the experiment and computational fluid dynamics (CFD) result of Aono et al. [14] using a Zimmerman wing prescribed with a single DOF flap rotation at the wing root. Figure 3 (b) shows that the amplitude and phase of the vertical displacement of wing tip normalized by the root chord are in reasonable agreement with the baseline experimental and CFD results [14]. The tip displacement shows good symmetric response between the up stroke and down stroke.

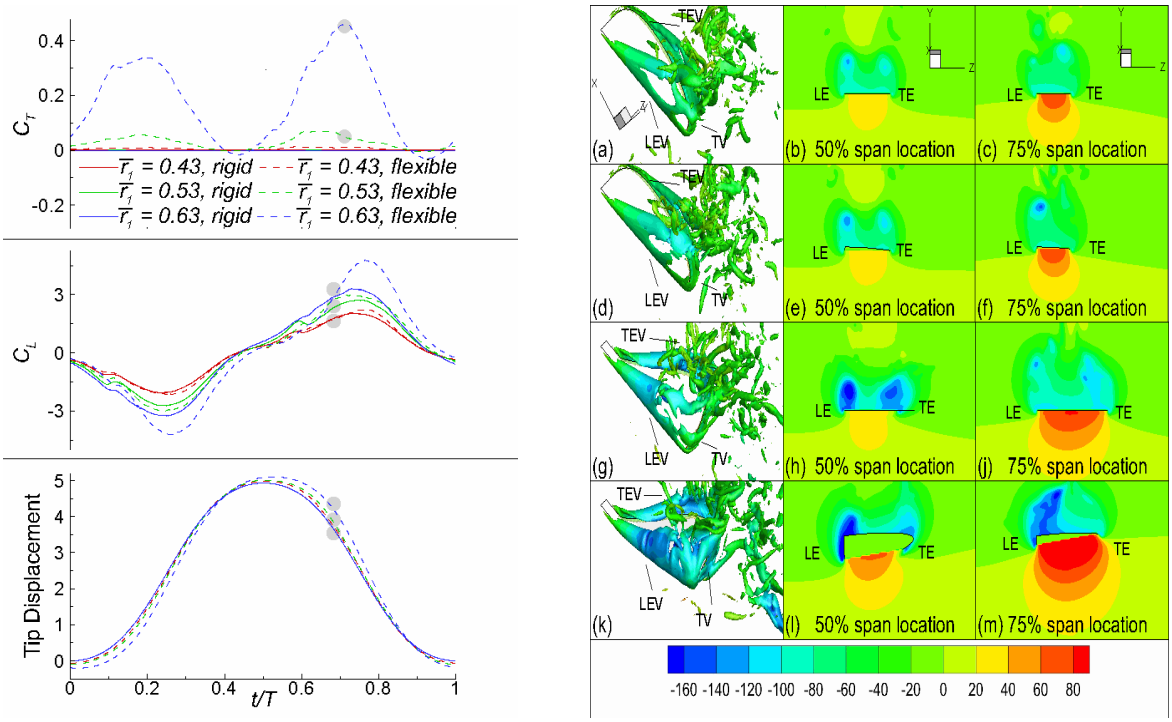

Figure 4. (Left) Time histories of C_T, C_L, and wing tip displacements of rigid and flexible wings . (Right) Iso-Q surfaces and pressure coefficients at t/T = 0.7: (a-c) $\bar{r}_1$= 0.43, rigid, (d-f) $\bar{r}_1$= 0.43, flexible (g-j) $\bar{r}_1$= 0.63, rigid and (k-m) $\bar{r}_1$= 0.63, flexible wing.

5. Results and discussions

This section includes the details of time history of force coefficients and wing tip displacement, and the flow features of rigid and flexible $\bar{r}_1$ = 0.43 and 0.63 wings at *t/T* = 0.7 (figure 4). For $\bar{r}_1$ = 0.43, the rigid (figure 4 (b) and (c)) and flexible wings (figure 4 (e) and (f)) show similar pressure coefficient distributions at 50% and 75% span locations. As a result, the C_T of flexible $\bar{r}_1$ = 0.43 wing, although non-zero, is very small. For $\bar{r}_1$ = 0.63, at the same spanwise locations, the pressure distributions of the rigid (figure 4 (h) and (j)) and flexible wings (figure 4 (l) and (m)) show marked differences. There is an induced pitch angle in the flexible wing that orients the pressures and resultant of the aerodynamic force for favourable thrust production. This indicates that, with more area distributed outboard towards the tip, the high $\bar{r}_1$ wing shows high chordwise flexibility in the distal part of the wing that result in higher thrust. At this time instant (*t/T* = 0.7), the flexible $\bar{r}_1$ = 0.63 wing produces the peak C_T. Like the thrust, the time history of C_L in figure 4 also shows that flexibility improves the peak lift and it increases with increasing $\bar{r}_1$. For $\bar{r}_1$ = 0.63 wing, there is a 30.3% increase in the peak lift with the introduction of flexibility and this peak is registered during the down stroke at *t/T* = 0.75, when the flapping velocity is maximum. Careful examination of the wing tip displacements in figure 4 shows that the flapping amplitude of the flexible wing increases and this increase is more pronounced for high $\bar{r}_1$ (3.4% increase for $\bar{r}_1$= 0.63 wing). Since the time period remains unchanged, the velocity is bound to increase with flexibility, and this in turn results in higher suction pressures and more lift. Although the flexible $\bar{r}_1$= 0.43 wing produces high peak lift than its rigid counterpart, their lift coefficients are similar at *t/T* = 0.7 as evident from the iso-Q surfaces of the rigid (figure 4 (a)) and flexible (figure 4 (d)) wings. For $\bar{r}_1$ = 0.63, the iso-Q surfaces of rigid (figure 4 (g)) and flexible (figure 4 (k)) wings show that the LEV on the rigid wing starts to break down (at approximately 60%) after the mid span. On the contrary, the spanwise deformation in the flexible wing anchors the LEV on the wing as it joins the tip vortex. This results in an increase in the peak lift because of flexibility. The degree of spanwise deformation in $\bar{r}_1$ = 0.43 and 0.63 wings can be observed in figure 5. While the flexibility in $\bar{r}_1$= 0.43 wing is small, there is significant deformation in the distal parts of the flexible $\bar{r}_1$= 0.63 wing.

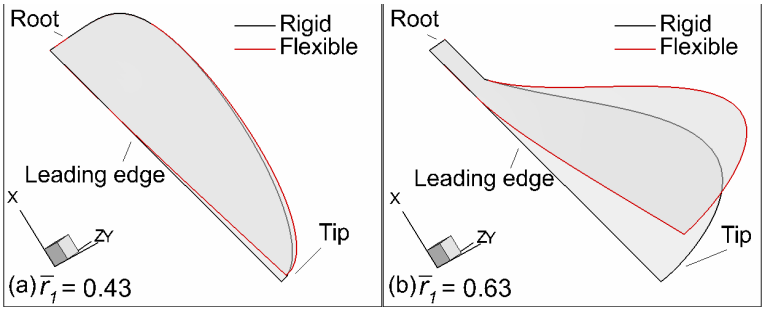

Figure 5. Spanwise deformation in flexible wings at *t/T* = 0.7.

6. Conclusion

Numerical simulations were performed at Re = 6000 using an IBM solver to compare the aerodynamic performance of rigid and flexible wing shapes. The results show that, while rigid wings do not produce any thrust, the flexible wings generate thrust whose magnitude and peak value increases with increasing $\bar{r}_1$ because high $\bar{r}_1$ wings induce pitch angles, which changes the orientation of the resultant aerodynamic force to produce more thrust. In addition, the peak lift forces of flexible wings are also higher than their rigid counterparts. This is because lift scales as the square of the wing tip velocity which increases with $\bar{r}_1$ due to an increase in the stroke amplitude (maximum of 3.4% increase in stroke amplitude in $\bar{r}_1$ = 0.63 wing). The spanwise deformation of flexible wings also anchors the LEV on the wing and contributes to more lift. Among flexible wings, $\bar{r}_1$ = 0.63 wing produces maximum

peak lift. In conclusion, flexibility plays a key role in defining the aerodynamic performance of wing shapes.

Acknowledgments
This work was supported under the Australian Research Council's Discovery Projects funding scheme (project number DP130103850), and was conducted with the assistance of resources from the National Computational Infrastructure (NCI), which is supported by the Australian Government. Aamer Shahzad acknowledges the support of NUST, Islamabad, Pakistan via the Prime Minister's Gold Medal Scholarship and SEIT, UNSW, Canberra, which provided a top-up scholarship.

References
[1] Phillips, N., Knowles, K. & Lawson, N., 2010, "Effect of wing planform shape on the flow structures of an insect-like flapping wing in Hover", *27th International Congress of the Aeronautical Sciences. ICAS. Nice, France*.
[2] Ozen, C. & Rockwell, D., 2013, "Flow Structure on a Rotating Wing: Effect of Wing Aspect Ratio and Shape", *51st AIAA Aerospace Sciences Meeting including the New Horizons Forum and Aerospace Exposition*. *Grapevine, Texas*.
[3] Luo, G. & Sun, M., 2005, "The effects of corrugation and wing planform on the aerodynamic force production of sweeping model insect wings", *Acta Mechanica Sinica*, 21(6), pp 531-541.
[4] Ansari, S.A., Knowles, K. & Zbikowski, R., 2008, "Insectlike flapping wings in the hover part II: Effect of wing geometry", *Journal of Aircraft*, 45(6), pp 1976-1990.
[5] Wilkins, P.C., 2008, "Some unsteady aerodynamics relevant to insect-inspired flapping-wing micro air vehicles", Cranfield University, UK.
[6] Shahzad, A., Tian, F., Young, J. & Lai, J., 2014, "Reynolds Number Effects on the Aerodynamic Performance of Wing Planform Shapes in Hover", *19th AFMC. RMIT University, Melbourne, Australia*.
[7] Ellington, C., 1984, "The aerodynamics of insect flight. II. Morphological parameters", *Phil. Trans. R. Soc. Lond. B*, 305, pp 17-40.
[8] Combes, S.A. & Daniel, T.L., 2003, "Flexural stiffness in insect wings I. Scaling and the influence of wing venation", *Journal of Experimental Biology*, 206(17), pp 2979-2987.
[9] Shyy, W., Aono, H., Kang, C.-k. & Liu, H., 2013, "*An introduction to flapping wing aerodynamics*", Vol 37, Cambridge University Press.
[10] Combes, S. & Daniel, T., 2003, "Flexural stiffness in insect wings II. Spatial distribution and dynamic wing bending", *Journal of Experimental Biology*, 206(17), pp 2989-2997.
[11] Tian, F.-B., Dai, H., Luo, H., Doyle, J.F. & Rousseau, B., 2014, "Fluid–structure interaction involving large deformations: 3D simulations and applications to biological systems", *Journal of Computational Physics*, 258, pp 451-469.
[12] Nagai, H., Isogai, K. & Fujimoto, T., 2010, "Experimental study on flow interaction between fore-and hindwings of dragonfly in hovering and forward flight", *27th Congress of International Council of the Aeronautical Sciences*. *Nice, France*.
[13] Naidu, V., Young, J. & Lai, J., 2013, "Effect of wing flexibility on the performance of tandem wings during hover flight", *31st AIAA Applied Aerodynamics Conference*. *San Diego, CA*.
[14] Aono, H., et al., 2010, "A computational and experimental study of flexible flapping wing aerodynamics", *48th AIAA aerospace sciences meeting including the new horizons forum and aerospace exposition*. pp. 4-7.